Tellus (1999), 51A, 233–248
Printed in UK – all rights reserved

TELLUS
ISSN 0280–6495

Potential vorticity-based interpretation of the evolution of "The Greenhouse Low", 2–3 February 1991

By JÓN EGILL KRISTJÁNSSON[1]*, SIGURDUR THORSTEINSSON[2] and GUDMUNDUR FREYR ULFARSSON[2], [1]*Department of Geophysics, University of Oslo, P.O. Box 1022 Blindern, N-0315 Oslo, Norway.* [2]*Icelandic Meteorological Office, Bústadavegi 9, IS-150 Reykjavík, Iceland*

(Manuscript received 12 November 1997; in final form 12 August 1998)

ABSTRACT

The explosive synoptic-scale "Greenhouse Low" that hit Iceland on 3 February 1991 has been examined in the potential vorticity (PV) framework. Three positive PV anomalies were investigated in detail: (1) a surface thermal anomaly, (2) a lower-tropospheric, diabatically produced PV anomaly, and (3) a PV anomaly propagating along the tropopause. Through PV piecewise inversions, we have quantified the contributions of these 3 anomalies to the total geopotential field. By using a specific, quasi-linear procedure, the total geopotential field can be retrieved from the sum of the mean field and all the PV anomalies (positive and negative). The piecewise inversions were performed at different times and for different simulations using HIRLAM. This allows us to draw a comprehensive picture of the time evolution of the cyclone, and to quantify the rôles played by different dynamical and physical processes. Initially, the surface thermal anomaly on the southeastern flank of the baroclinic region was crucial in spinning up the cyclone. Latent heating in the lower troposphere due to frontal ascent then took over as the most important contributor to cyclone deepening. The associated PV anomaly intensified explosively between 06 UTC 2 February and 00 UTC 3 February. The upper-level PV anomaly also played an important role, especially in the later stages, between 06 and 12 UTC 3 February. Our findings suggest that this anomaly was mainly a separate entity that influenced the low-level flow, but was partly due to vertical propagation of PV from the lower layers.

1. Introduction

The area around Iceland is one of the most favoured regions in the world for cyclonic activity. This includes both synoptic-scale cyclones and meso-cyclones, e.g., polar lows. This large activity is caused by several factors, including strong gradients in sea-surface temperature and orographic effects due to Greenland. A series of studies is currently under way, aimed at a better understanding of the causes for different types of cyclones in this region, as well as the role of dynamical and physical processes in their development.

In the first of these studies, the so-called Greenhouse Low of 2–3 February 1991 was investigated through a combination of model simulations and careful re-analysis of surface observations and satellite data (see Kristjánsson and Thorsteinsson 1995, hereafter KT). The cyclone was not unusually deep but it was characterized by strong pressure gradients and hurricane-force winds, making it one of the most destructive storms to hit Iceland in this century. The measured pressure tendency reached +30.4 hPa/3h at one station (KT). We now return to this same cyclone, using the potential vorticity (PV) perspective (Hoskins et al. 1985) to investigate the cyclone evolution in more detail. Using a method recently developed by Davis and Emanuel (1991), hereafter DE, and Davis (1992), we perform piecewise PV

* Corresponding author.

inversions under nonlinear balance conditions to *quantify* and to determine objectively the relative importance of different portions of the PV field for the evolution. The method of Davis (1992) ensures that the total height field can, to a good approximation, be partitioned into contributions from the mean field and from the PV anomalies (including the potential temperature anomalies at the horizontal boundaries). By combining this procedure with the results of the sensitivity experiments described by KT, we can deduce a comprehensive picture of the rôle of different mechanisms in the evolution of the cyclone. In addition to the main positive anomalies we also investigate the major negative anomalies needed to avoid large residues.

In the last few years, many authors have used PV diagnostics in various forms to assess different aspects of extratropical cyclones. For instance, Grønås (1995) showed how a traveling upper-level PV anomaly first created an explosive cyclone in the North Atlantic, and then how a low-level PV anomaly, created by latent heat release, caused an intense back-bent frontal development, which contributed strongly to the devastating winds that occurred. The PV-inversion technique developed by DE and Davis (1992) has previously been used by Davis et al. (1993) and Stoelinga (1996) to quantify the rôles of diabatic and frictional processes in explaining explosive cyclogenesis off the east coast of North America. Recently, Wu and Emanuel (1995a, 1995b) presented results from investigations of hurricane movement using the methodology of DE and Davis (1992).

The diagnostic methods used in this study are described in Section 2. The synoptic description as well as analysis of the evolution and structure of the cyclone have been presented by KT, and will only be briefly reviewed at the beginning of Section 3. Further, Section 3 describes the results of applying the PV diagnostics method to our case, giving the time evolution of the various PV features during the cyclone's life cycle. Following an assessment of the methodology and the results in Section 4, the conclusions are stated in Section 5.

2. Potential vorticity diagnostics

2.1. Background

The significance of potential vorticity (PV) as a diagnostic quantity in meteorology is largely due to its conservation properties. As shown originally by Rossby (1940), PV is conserved following the motion of a particle in adiabatic, frictionless flow. This leads to many interesting effects. First, following Ertel (1942), we define PV as:

$$q = \frac{1}{\rho} \boldsymbol{\eta} \cdot \nabla\theta . \tag{1}$$

Here ρ denotes density and $\boldsymbol{\eta}$ is the absolute vorticity vector in 3 dimensions, while θ is potential temperature. It follows from (1) that air descending from the stratosphere, where the static stability is large, will tend to acquire cyclonic vorticity as it enters the troposphere, where the stability is much weaker, due to the conservation of PV. As pointed out by Hoskins et al. (1985) this can have large implications for cyclone deepening, since tropopause foldings with associated descent of air from the stratosphere to the troposphere are indeed an observed feature of many synoptic-scale cyclones (Reed, 1955; Shapiro, 1970; Uccellini, 1990).

2.2. The PV inversion system

We shall here briefly review the basic equations from DE. First we express a very important aspect of PV, namely the "invertibility principle" which states that, given appropriate balance requirements as well as boundary conditions, all the dynamical fields can be uniquely obtained from the PV field. Following DE, equation (1) can be rewritten in spherical coordinates, after performing scale analysis, as:

$$q = \frac{g\kappa\pi}{p} \left[(f + \nabla^2\Psi) \frac{\partial^2\Psi}{\partial\pi^2} - \frac{1}{a^2 \cos^2\phi} \times \frac{\partial^2\Psi}{\partial\lambda\,\partial\pi} \frac{\partial^2\Phi}{\partial\lambda\,\partial\pi} - \frac{1}{a^2} \frac{\partial^2\Psi}{\partial\phi\,\partial\pi} \frac{\partial^2\Phi}{\partial\phi\,\partial\pi} \right] . \tag{2}$$

Here λ denotes longitude, ϕ latitude, f is the Coriolis parameter, g the gravitational acceleration and a is the radius of the earth, while π denotes the Exner function ($c_p T/\theta$), p is pressure and $\kappa = 0.286$. The geopotential is given as Φ, and the non-divergent streamfunction as Ψ. The only requirement for obtaining the dynamical fields from the PV field is a proper inversion algorithm. Recently DE devised such an algorithm, using the non-linear balance equation of Charney (1955) to supply the relation between the Ψ and Φ fields:

$$\nabla^2\Phi = \nabla\cdot(f\nabla\Psi) + \frac{2}{a^4\cos^2\phi}\frac{\partial}{\partial(\lambda,\phi)}\left(\frac{\partial\Psi}{\partial\lambda},\frac{\partial\Psi}{\partial\phi}\right), \tag{3}$$

the last term being the Jacobian. This non-linear balance condition is capable of handling a flow with large curvature, as long as it remains inertially stable.

Boundary conditions are as follows. At the lateral boundaries the analyzed geopotential and streamfunction on the boundary are used. On the horizontal boundaries the conditions are $\partial\Phi/\partial\pi = -\theta$ and $\partial\Psi/\partial\pi = -\theta/f$. To perform the PV inversion, i.e., to solve equations (2) and (3) for the height and streamfunction, we also need the appropriate PV and θ fields, along with initial guesses for the geopotential. From the geopotential fields, a first-guess streamfunction field is obtained from the quasi-geostrophic assumption:

$$\Psi^0 = \frac{\Phi}{f}. \tag{4}$$

A successive overrelaxation method (SOR) is used to solve the system (2)–(4). Note that the equations are not balanced if q is negative, and the method, therefore, can not adequately describe fields in an area of negative PV.

2.3. *Model and data*

This study was carried out using the HIRLAM (HIgh Resolution Limited Area Model) model system, described in detail by Gustafsson (1993). HIRLAM is a hydrostatic, primitive equation, finite-difference model that is used for operational weather predictions in several countries in northern Europe. In our setup the model has a horizontal grid spacing of 0.5 degrees in a rotated Gaussian grid, corresponding to a resolution of about 55 km. In the vertical there are 16 levels, determined by a hybrid vertical coordinate, which acts similarly to sigma in the lower troposphere, but approaches a constant pressure coordinate above. The input data used in this investigation are the European Centre for Medium Range Weather Forecasts (ECMWF) uninitialized analyses, available every 6 h. The analyses of potential temperature and geopotential height given at the mandatory levels* were then used to compute PV on pressure surfaces according to the centered finite-difference analogue of equation (2). Thus, PV is obtained at mandatory levels, ranging from 900 to 150 hPa. Potential temperature at 950 hPa (1000–900 hPa average) and at 125 hPa (150–100 hPa average) is used for the lower and upper boundary conditions, respectively.

Clearly, the use of θ as a vertical coordinate would have simplified the PV analysis, in that equation (2) then reduces to only one term, since the horizontal derivatives of θ vanish and adiabatic flow becomes purely two-dimensional. Such isentropic PV analysis have been carried out by many investigators, e.g., Davis et al. (1993), Grønås (1995). However, in a model setup like ours the disadvantage of having to carry three terms for PV is negligible, and we retain the convenience of using standard pressure levels instead of the somewhat cumbersome isentropic surfaces. A similar argument was presented by Reed et al. (1992).

2.4. *PV and θ anomalies*

A variant of the piecewise PV inversion method in DE is used to quantify the interactions between isolated portions of the fluid. The procedure requires a separation into a time mean state and an arbitrary number of PV anomalies. We define a *time mean state* PV field as $\bar{q}$ and a perturbation PV field as q', such that

$$q_{\text{tot}} = q(\lambda,\phi,\pi,y) = \bar{q}(\lambda,\phi,\pi) + q'(\lambda,\phi,\pi,t), \tag{5}$$

and do the same for θ:

$$\theta_{\text{tot}} = \theta(\lambda,\phi,\pi,t) = \bar{\theta}(\lambda,\phi,\pi) + \theta'(\lambda,\phi,\pi,t). \tag{6}$$

A PV anomaly (q_i) is a part of the perturbation field denoted by q' in equation (5) through:

$$q' = \sum_{i=1}^{n} q_i. \tag{7}$$

where n stands for the total number of anomalies in the perturbation field. We shall now describe how the piecewise inversion was performed. In this section we will write a few descriptive relations between the fields and normally only write the

* These levels are: 1000, 900, 800, 700, 600, 500, 400, 300, 250, 200, 150, 100 hPa.

relations for the q fields, but similar relations hold for θ as well.

First a subjective evaluation of the PV field is carried out, and conspicuous PV features are singled out as anomalies of interest (see Subsection 3.4.1). We then *invert* PV piecewise. Davis (1992) explored different methods of performing the piecewise inversion. Based on his findings, we chose to combine the two methods that he termed ST (subtraction from total) and AM (addition to the mean). According to Davis (1992) the average of the resulting fields from these two methods gives results very similar to a linearized method used by DE, which Davis (1992) termed FL (full linear). This linearization analogy implies that we can, to a good approximation, add the geopotential fields corresponding to the anomalies, residual and average PV and θ fields, to obtain the total geopotential field. Note that this represents an improvement over inversion techniques based on quasi-geostrophic potential vorticity (QGPV) (Hakim et al. (1996)), since we have retained a more general form of PV than QGPV is.

We now calculate the cumulative effect of the anomalies not explicitly removed, that is, the anomalies with $i=N+1, \ldots, n$. This residual field can be written as:

$$q_{\text{res}} = \sum_{i=N+1}^{n} q_i \,. \tag{8}$$

The calculation is carried out in a manner analogous to that for the isolated anomalies.

Finally, having performed all the inversions, we evaluate how well the different terms contributing to the total geopotential field add up. This is done by computing "an error term", $\Delta\Phi$, which is defined by the equation:

$$\Delta\Phi = \Phi_{\text{tot}} - \bar{\Phi} - \sum_{i=1}^{N} \Phi_i - \Phi_{\text{res}} \,. \tag{9}$$

In the inversions performed in this study the average absolute value of the height error, obtained by dividing $\Delta\Phi$ by g, was 6.3 m (see "error" in Tables 1–5). Based on this small error we conclude that we can confidently compare the contributions from the different PV anomalies to the total flow, based on the results from the inversion calculations.

3. Piecewise PV inversions applied to the 2–3 February 1991 cyclone

3.1. *Synoptic overview*

The synoptic conditions in the lower troposphere are indicated in Figs. 1a–c, which show the analyzed height field at 900 hPa at 18-h intervals, together with 900 hPa potential temperature and upper level potential vorticity. In (a) the low-level cyclogenesis is just about to start near the lower left hand corner of the figure. As the cyclone starts to deepen (b), we see strong temperature advection at low levels, while the upper level potential vorticity anomaly (shaded) starts approaching the cyclone, as discussed by KT. This suggests cyclone deepening by both low-level and upper-level processes acting together. The "merging" of the two systems, suggested by Figs. 1c and 2, will be investigated in some detail.

3.2. *PV partitioning*

The findings of KT suggested that three significant and dynamically distinct anomalies could be identified: A positive PV anomaly propagating along the tropopause, an anomaly associated with the surface baroclinicity, and a positive lower-tropospheric PV anomaly produced mostly by latent heat release due to condensation. We define the 3 positive anomalies as follows: (a) *surface* θ', a 950 hPa potential temperature anomaly. A positive *surface* θ' is equivalent to a positive PV anomaly (Hoskins et al. 1985). *Surface* θ' is normally created by warm and cold advection in the lower troposphere during baroclinic wave growth. Surface fluxes of heat can also contribute to this quantity. (b) LPV, a positive low-level PV anomaly (below 550 hPa). In the real atmosphere, latent heat release leads to the formation of positive PV anomalies at low levels and negative PV anomalies at upper levels, as seen from the equation

$$\frac{\mathrm{d}}{\mathrm{d}t}(q) = q^2 \frac{\mathrm{d}}{\mathrm{d}\theta}\left(\frac{\dot{\theta}}{q}\right), \tag{10}$$

from Hoskins et al. (1985); see also, e.g., Fig.4 by Wernli and Davies (1997). In a dry atmosphere, LPV can be created only by advection if there is a lower tropospheric gradient of PV on isentropic surfaces. (c) UPV, a positive upper-level PV anomaly (above 550 hPa). This anomaly is typically related to a lowering of the tropopause in a cold air mass. The three positive PV anomalies are indicated by solid frames in Fig. 4, while the dotted and dashed frames depict negative anomalies explained below.

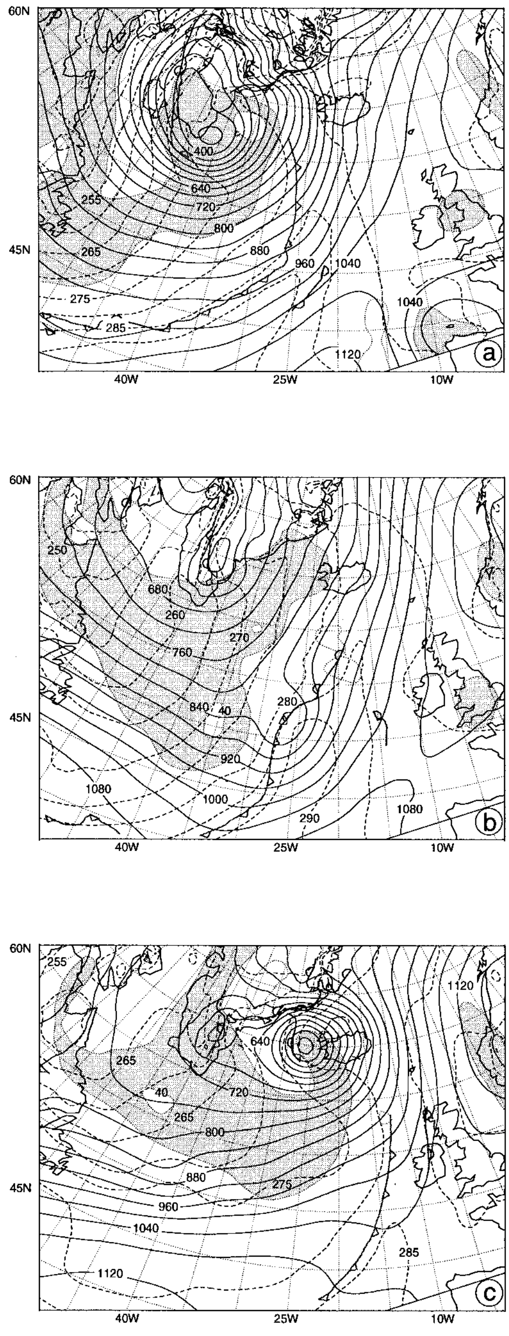

Fig. 1. Analyzed 900 hPa height field (solid lines) and potential temperature field (dashed lines) at 900 hPa at: (a) 00 UTC 2 February 1991; (b) 18 UTC 2 February 1991; (c) 12 UTC 3 February 1991. The shaded areas correspond to 40 dPVU ⩾ PV ⩾ 20 dPVU on 400 hPa (1 dPVU = 0.1 PVU). The fronts shown are objectively analyzed from the gradient of 850 hPa equivalent potential temperature (also in Figs. 2, 4, 6, 8, 9 and 10).

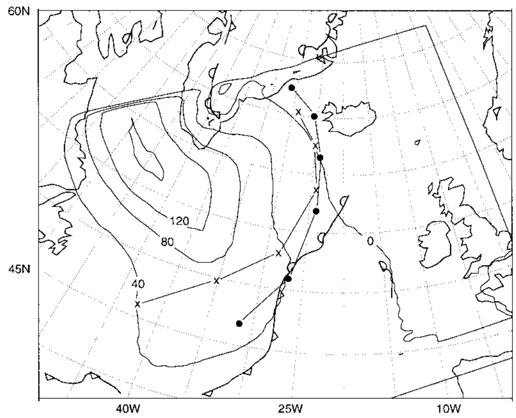

Fig. 2. The upper level (×) and surface cyclone (●) track (every 6 h between 12 UTC 2 February and 18 UTC 3 February) and the difference in geopotential height (in m) between the original and the balanced 900 hPa height fields at 18 UTC 2 February 1991.

The choice of 550 hPa as a dividing line between upper and lower level anomalies was based on investigations of the vertical extent of the anomalies. We then selected the 2 layers with the strongest anomalies. This led to the choice of 400 hPa as a representative level for the upper level anomaly and 900 hPa as representative for the lower level anomaly.

Having performed the inversions we shall focus on the impact of the anomalies on the 900 hPa height field. The reason for choosing the 900 hPa level is that this is the lowest model level above the lower boundary (see location of pressure levels in Subsection 2.3).

3.3. *PV inversions*

The mean 400 hPa PV, 900 hPa PV and 950 hPa potential temperature used for the inversion procedure are shown in Figs. 3a, b and c, respectively. Here the mean state is defined as either the time-average over the 42 hour period

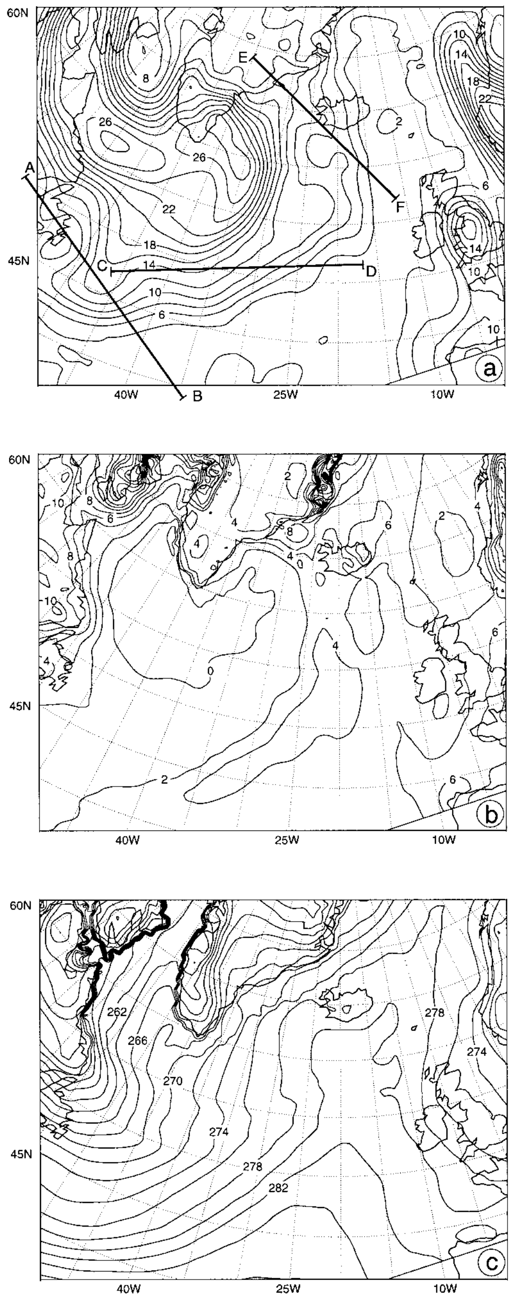

Fig. 3. 42-h mean: (a) PV (in dPVU) at 400 hPa; (b) PV (in dPVU) at 900 hPa; (c) lower boundary $\bar{\theta}$ (K) at 950 hPa (1 dPVU = 0.1 PVU).

00 UTC 2 February — 18 UTC 3 February 1991 or in some cases the time-average over the 24-h period 12 UTC 2 February — 12 UTC 3 February 1991 (Subsection 3.4). The suitability of the time mean for defining PV and θ anomalies has been demonstrated by DE. Assuming (see Hoskins and Berrisford, 1988) that the tropopause can be defined as a surface with PV = 20 dPVU (1 dPVU = 0.1 PVU), Fig. 3a indicates an intrusion of stratospheric air at 400 hPa over a fairly large region west of the cyclone track, shown in Fig. 2. The temporal movement of the high-PV air aloft is indicated by the crosses, which give the position of maximum 400 hPa PV at 6-h intervals.

In performing the inversion computations described above on the original grid, certain convergence problems were encountered. To overcome these convergence problems, as well as to speed up the convergence, the grid spacing was increased by a factor of 4 in both x and y directions, from 55 km to 220 km. The PV inversion was first performed on this coarse grid. Subsequently a local bi-cubic interpolation was used to interpolate the coarse grid height and streamfunction to a grid spacing of 110 km for use as the first guess in a second inversion step performed on this finer grid. Finally, a local bi-cubic interpolation was again used to interpolate to a horizontal resolution of 55 km. These are our presented values for the height and the streamfunction. The reason for these convergence problems is not fully clear but the difficulties tend to start within areas of negative potential vorticity, where, as mentioned in Subsection 2.2, the balance requirements needed for a proper inversion are not satisfied. Such an area is found to the south and southwest of Greenland, where cold advection, accompanied by heating from the warm ocean surface below, leads to negative PV values (through the $\partial\theta/\partial\pi$ term in (2)) over a large region south of Greenland (Fig. 3b).

In Fig. 2, we show the difference between the balanced solution of the full field and the actual heights of the same field for 18 UTC 2 February. As seen we find mostly rather small differences, usually much less than 40 gpm at 900 hPa. The exception is the statically unstable region discussed above, where considerably larger discrepancies were found. Fortunately that area is far enough away from the center of the cyclone that it should not affect the low-level circulation associated with it. Differences in wind speed between analyzed and balanced nondivergent fields (not shown) are found to be generally smaller than 5 m s^{-1}.

3.4. Results from the PV inversions

3.4.1. Evolution of the PV anomalies. To facilitate the understanding of the various aspects of cyclone dynamics dealt with here, we shall accompany analysis fields with results from different model simulations, as in the previous study by KT: CONTROL = simulation starting at 12 UTC 2 February 1991, using ECMWF analysis at the boundaries; NOLAT = as CONTROL, except that latent heat of condensation is omitted in the thermodynamic energy equation; RUN00 = as CONTROL, except starting at 00 UTC 2 February 1991.

Shown in Fig. 4 is the evolution of the 400 and 900 hPa PV perturbation fields, as well as the θ' perturbation field. Note that the UPV, LPV and *surface* θ' anomalies (explained in Subsection 2.2) only contain positive values within the rectangles shown. Figs. 4a–c show the dry 400 hPa PV anomaly of interest (the UPV anomaly) as a rather well defined zone of PV ≈ 2.0 PVU or more, moving ENE originally and later NNE. At the final time shown it is almost vertically aligned with the surface cyclone, but with an elongation to the southwest. The 900 hPa PV anomaly (Figs. 4d–f) originates largely from latent heat release, as will be demonstrated below (based on results from NOLAT). It has a very different evolution from that of the 400 hPa anomaly, having small amplitude at the initial time (Fig. 4d), but then gaining strength in the developing phase of the cyclone (Fig. 4e), reaching more than 1 PVU at the final time (Fig. 4f). It is also found (not shown) that the low-level anomaly coincides with large relative humidities, as is required for latent heat release to take place.

The *surface* θ' perturbation, shown in Figs. 4g–i, mainly consists of a positive anomaly, located just on the warm side of the surface low and a negative anomaly behind the cold front to the west and northwest of the surface low. The positive anomaly reaches its largest magnitude at the initial time, exceeding 8 K (Fig. 4g). At 18 UTC 2 February (Fig. 4h) and 12 UTC 3 February (Fig. 4i) it is located in the warm sector of the cyclone and with maximum amplitudes of about 5 K and 4 K, respectively. The areal extent of this anomaly decreases during the cyclone evolution, while that of the cold anomaly increases, as the warm air rises and cold air is brought down, hence converting available potential energy to kinetic energy of the disturbance.

To get a better picture of the three-dimensional aspects of the PV evolution, we show in Figs. 5a–c cross-sections of PV from the CONTROL run. Assuming that the tropopause can be defined by a sharp increase in the vertical gradient of PV (Shapiro and Keyser, 1990; Hoskins and Berrisford, 1988), we see a gradual lowering of the tropopause above the surface cyclone, as time progresses. At the initial time (Fig. 5a) the low-level PV is very weak, but during the later stages of the cyclone's development a region of significant low-level positive PV values is created, especially below 600 hPa (Fig. 5b–c). It is not clear a priori whether the vertical alignment of large PV values above the cyclone in Fig. 5c is due to constructive interference by two independent phenomena, i.e., an upper and a lower level PV-anomaly, or is caused by vertical propagation of low-level PV in the untilted occluded cyclone. We shall return to this question in Subsection 3.4.4. The negative PV-values at the upper right corner of Fig. 5a are due to negative absolute vorticity in this region.

3.4.2. Contributions to cyclone deepening. We shall now look at the contributions to the 900 hPa geopotential height fields from the three main PV anomalies. We first focus on results obtained using model analyses. In Figs. 6a–c, we see the contribution from UPV at three different times, while Figs. 6d–f show the corresponding result for LPV, whereas Figs. 6g–i display the contribution from *surface* θ'.

In addition to the change with time of the relative strength of the three anomalies, which will be discussed in more detail below, we also see interesting phase differences: The UPV signature is consistently farther upstream than the other two, although somewhat less so as time progresses. Conversely, the *surface* θ' anomaly tends to deepen the low in the direction of the warm air on its downstream flank. The LPV contribution is most closely in phase with the actual surface low, indicated by "L" in the figure. Figs. 6j–l show the contribution from the residual field at 900 hPa. Note that for the time being all negative PV

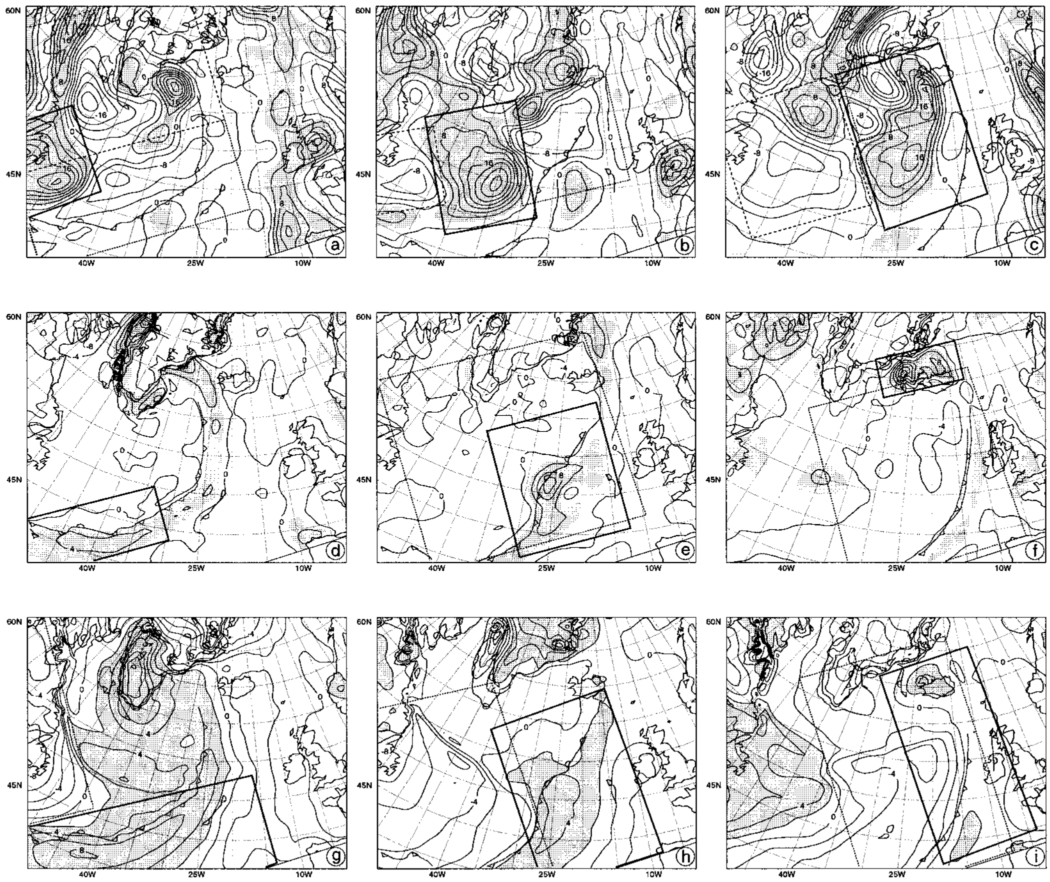

Fig. 4. Perturbation fields associated with 400 hPa PV (in dPVU, top row), 900 hPa PV (in dPVU, middle row) and lower boundary θ (in K, bottom row). The anomalies UPV, LPV and *surface* θ' are defined as positive values within the indicated solid rectangles. The shaded areas in the top and middle row correspond to $q' > 2$ dPVU, while in the bottom row they indicate $\theta' > 2$ K. Negative anomalies are dotted, except UPVN2 which is dashed. Left column is for 00 UTC 2 February, middle column for 18 UTC 2 February, and right column for 12 UTC 3 February.

anomalies are contained in the residual field. The residual field contributes significantly to the weakening of the low over the first 24 h or so, but from then on its effect near the low center is gradually reduced (Table 1). At the final time (Fig. 4l) its impact is largest to the rear of the surface cyclone (Fig. 6l), which corresponds well with the filling given by negative *surface* θ' (Fig. 4i).

Due to the choice of only three PV anomalies, all of which were positive, we obtained in Fig. 6 a fairly large residual term, representing mostly anticyclonic circulation. How does this affect the interpretation of the height fields from the three PV anomalies? We shall deal with this issue more directly in Section 4, but a partial answer to the question is given by Fig. 7, which shows the sum of the geopotential heights from, respectively, the residual field and the upper-level PV anomaly at the time when we expect the upper-level PV anomaly to be most important. We see that despite the large positive height values associated with the residual term, there still remains a strong cyclonic depression, when the UPV height field is added. The geopotential height of this cyclone is about -125 m, its position being shifted slightly to the southeast of the analyzed cyclone, Fig. 1. We may thus conclude that the UPV anomaly is

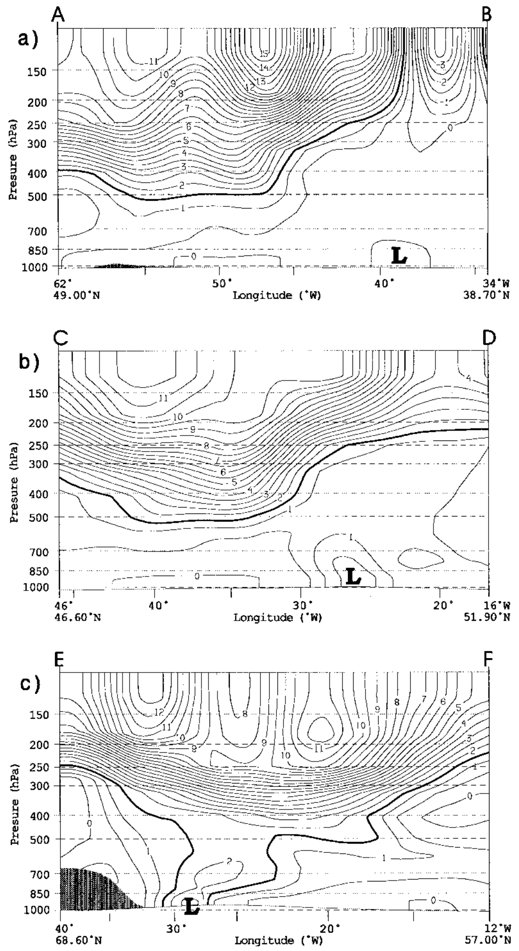

Fig. 5. PV cross sections from CONTROL: (a) at 00 UTC 2 February 1991; (b) at 18 UTC 2 February 1991; (c) at 12 UTC 3 February 1991. The line PVU = 1.5 has been enhanced for clarity (locations of cross sections are shown in Fig. 3a).

large enough not to be obscured by the negative PV anomaly associated with the residual term.

Tables 1–5 summarize the contributions to 900 hPa height at the cyclone center for different model runs every 6 h. Considering first the geopotential heights from the analysis data (Table 1), we see, as in Fig. 4, a systematic change in the role of the three anomalies as time evolves. The *surface* θ' anomaly gives by far the largest contribution of the three at the initial time, and remains very significant over the next 12 h. Over the final 24 h, however, the surface θ' anomaly weakens and its role is gradually overwhelmed by the contributions from the other two anomalies, UPV and LPV. The LPV anomaly is very weak at 00 and 06 UTC 2 February. At 12 UTC 2 February its contribution has become as large as that of the other two anomalies, and after that it continues to increase, except during the last 6 h, when the cyclone has reached maturity. The contribution of the upper level anomaly is already quite large at 06 UTC 2 February. From then on it grows quite slowly, apart from the final 6 h, when it grows rapidly, reaching its highest value at 12 UTC 3 February.

Table 2 shows results analogous to those in Table 1, except that the averaging is now done over the final 24 h only. Qualitatively, the main features are the same as in Table 1, the largest difference being found in the contribution from UPV, which is on average weaker by 17 gpm for the 24-h average than for the 42-h average.

We shall now compare Table 2 to sensitivity experiments with the HIRLAM model, using the analysis at 12 UTC 2 February as initial data. Table 3 shows results from the CONTROL simulation. They show a large similarity to those of the analyses, hence justifying the use of results from CONTROL in the assessment of the cyclone development, as done in KT. The most significant discrepancy is a slightly too weak contribution from UPV, while minor discrepancies associated with LPV and *surface* θ' have varying signs.

In KT we showed that omitting latent heat release led to a significantly weaker simulated cyclone. This result can be understood if we compare Table 4 to Table 3. After only 6 h, i.e., at 18 UTC 2 February, the height associated with LPV is 69 gpm higher in NOLAT than in CONTROL. 6 h later the difference has increased to 117 gpm. At the same time the height associated with UPV is now 27 m lower than in CONTROL. This trend continues, and after 24 h, at 12 UTC 3 February, the differences corresponding to LPV and UPV are +143 gpm and −57 gpm, respectively. This dipole structure is compatible with the notion that diabatic heating creates positive potential vorticity below the level of heating and negative potential vorticity above the level of heating, as discussed in Subsection 3.2. The fact that the height anomaly corresponding to LPV in NOLAT is quite small, apart from the first 6 h (Table 4), confirms the claim already made that the LPV

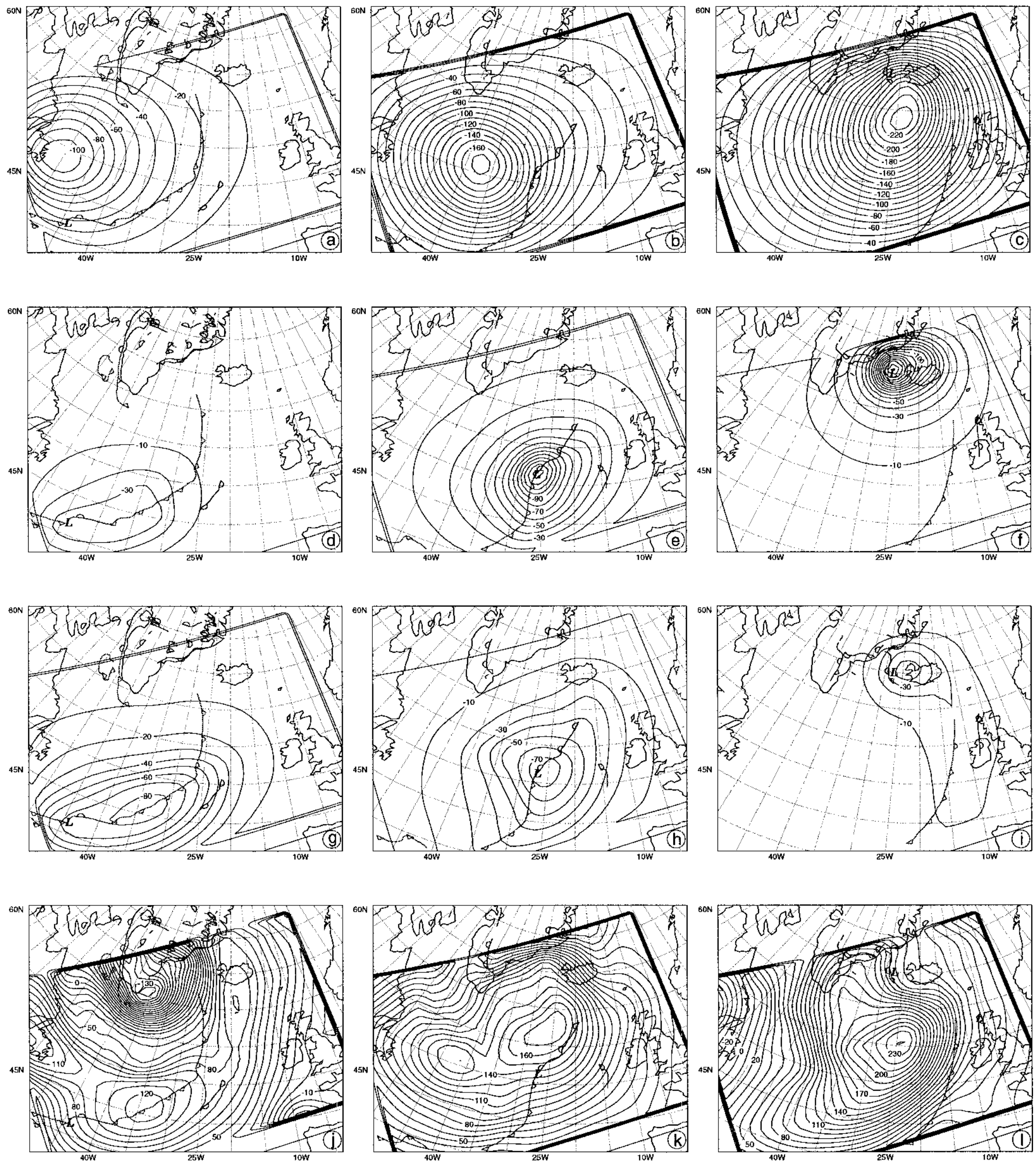

Fig. 6. Contributions to perturbation heights (in gpm) at 900 hPa from upper PV (q at 500 to 250 hPa, top row), lower PV (q at 900 to 600 hPa, upper middle row), lower boundary θ (lower middle row), and the residual field (bottom row), based on analyses. The position of the surface low center is denoted by L. Left column is for 00 UTC 2 February, middle column for 18 UTC 2 February, and right column for 12 UTC 3 February.

anomaly is largely a result of latent heat release. This is demonstrated in Fig. 8, which shows the LPV contribution to 900 hPa height fields for the two cases, CONTROL and NOLAT, at +18 h. At all times the contribution of the *surface* θ' anomaly is similar in NOLAT and CONTROL, i.e., displaying a systematic decrease with time.

3.4.3. Sensitivity to the initial state. Finally, we will investigate the sensitivity to the initial state

Table 1. *Contributions to geopotential height (in m) at 900 hPa at the location of the surface cyclone, from different anomalies at 6 h intervals, based on model analyses; a 42-h average from 00 UTC 2 February to 18 UTC 3 February was used.*

Contributions to geopotential height in 42 h analysis							
Date/time	2/00	2/06	2/12	2/18	3/00	3/06	3/12
total	967	915	852	751	668	568	444
mean	1051	1009	980	918	851	765	720
perturbation	−84	−94	−128	−167	−183	−197	−276
UPV	−35	−91	−82	−102	−108	−118	−181
LPV	−35	−45	−96	−133	−177	−173	−156
surface-θ′	−73	−61	−81	−75	−67	−39	−42
residual	67	107	124	137	169	138	98
error	−8	−4	7	6	0	−5	5

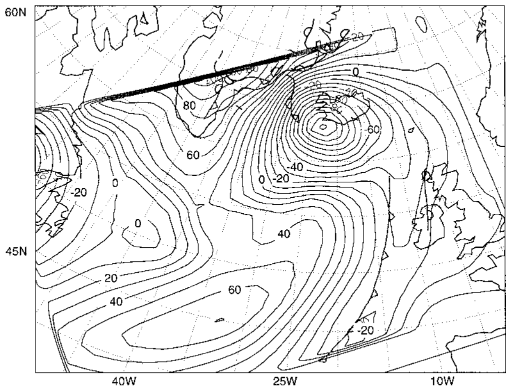

Fig. 7. The sum of geopotential heights at 900 hPa associated with the residual term and the upper-level potential vorticity anomaly at 12 UTC 3 February 1991.

by comparing the results from RUN00 to those of the other simulations. As explained in KT, RUN00 had large errors in both the positioning and the intensity of the cyclone, similar to those of many operational models at the time. Through this comparison we wish to answer the following two questions.

(1) Why did the RUN00 simulation fail to deepen and position the cyclone correctly, as opposed to CONTROL?

(2) Is the upper-level anomaly truly a separate entity that influences the low-level flow, or is it strongly affected by what happens at low levels?

To answer the first question, we first look at the contribution from the *surface θ′* anomaly at 12 UTC 2 February, since it was suggested in KT (Fig. 10 of that paper) that at this time the low-level contribution was much weaker in RUN00 than in CONTROL. Fig. 9 confirms this hypothesis by showing a much stronger cyclone resulting from the *surface θ′* anomaly in Fig. 9a than in Fig. 9b. The stronger cyclone will in turn give rise to stronger warm advection ahead of the low and stronger cold air advection to the rear of the low, as seen by assuming approximately geostrophic winds and holding Fig. 9 together with the potential temperature field in Fig. 3c. Through the omega equation (Holton, 1992), this gives rise to vertical motions that further intensify the cyclone in CONTROL, as compared to RUN00, due to baroclinic energy conversion.

Table 2. *As Table 1, except that a 24 h average from 12 UTC 2 February to 12 UTC 3 February was used*

Contributions to geopotential height in 24-h analysis					
Date/time	2/12	2/18	3/00	3/06	3/12
total	852	751	668	568	444
mean	968	890	821	750	723
perturbation	−116	−139	−153	−182	−279
UPV	−76	−73	−76	−109	−170
LPV	−102	−138	−171	−170	−163
surface-θ′	−118	−94	−64	−30	−41
residual	172	161	159	133	88
error	8	5	−1	−6	7

Table 3. *As Table 2, except based on CONTROL run*

Contributions to geopotential height in CONTROL					
Date/time	2/12	2/18	3/00	3/06	3/12
total	852	741	628	529	416
mean	968	890	821	769	724
perturbation	−116	−149	−193	−240	−308
UPV	−76	−68	−69	−120	−151
LPV	−102	−149	−187	−179	−157
surface-θ′	−118	−101	−77	−44	−35
residual	172	166	145	114	37
error	8	3	−5	−11	−2

Table 4. *As Table 2, except based on NOLAT run*

Contributions to geopotential height in NOLAT					
Date/time	2/12	2/18	3/00	3/06	3/12
total	852	796	742	661	605
mean	968	893	840	769	726
perturbation	−116	−97	−98	−108	−121
UPV	−76	−77	−96	−151	−208
LPV	−102	−80	−70	−23	−14
surface-θ′	−118	−87	−62	−29	−22
residual	172	145	136	108	134
error	8	2	−6	−13	−11

Table 5. *As Table 1, except based on RUN00*

Contributions to geopotential height in RUN00							
Date/time	2/00	2/06	2/12	2/18	3/00	3/06	3/12
total	967	943	892	819	745	688	615
mean	1051	1014	978	944	896	841	799
perturbation	−84	−71	−86	−125	−151	−153	−184
UPV	−35	−61	−78	−72	−73	−91	−126
LPV	−35	−41	−90	−134	−144	−153	−142
surface-θ′	−73	−72	−60	−63	−60	−32	−18
residual	67	104	137	141	134	137	114
error	−8	−1	5	3	−8	−14	−12

Comparing the *surface* θ' contributions in Tables 3 and 5 we see at 12 and 18 UTC 2 February a difference of 58 and 38 gpm respectively, while the difference in the contributions from UPV and LPV at these times is fairly small. This underlines the rôle of the low-level baroclinicity at the early stages. 6 h later, at 00 UTC 3 February, the largest difference between Tables 3 and 5 is in the LPV contribution, while at the two final times, 06 and 12 UTC 3 February, the largest difference is associated with the UPV contribution. This seems to suggest a vertical propagation of a PV anomaly as the cyclone deepens. Indeed, an estimate of the vertical propagation velocity can be carried out, yielding:

$$\omega \approx \frac{-500\ \text{hPa}}{18\ \text{h}}, \tag{11}$$

$$\downarrow$$

$$w \approx -\frac{\omega}{\rho g} \approx 0.08\ \text{m s}^{-1}. \tag{12}$$

This is indeed a reasonable vertical velocity within the cyclone, suggesting that such a vertical propagation of PV may have occurred. This could happen, e.g., through vertical advection (in the p-coordinate) in connection with the cold conveyor belt and the associated back-bent warm

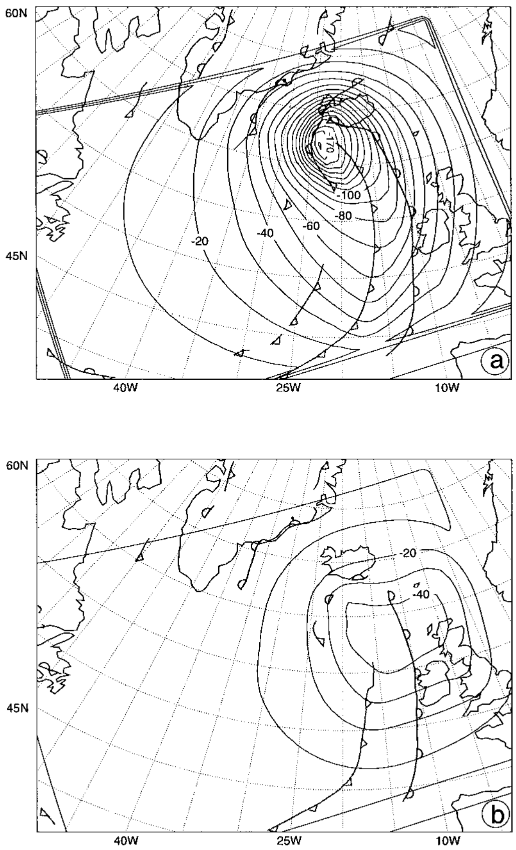

Fig. 8. Geopotential height field at 900 hPa associated with the low level PV anomaly (900 to 600 hPa) at 06UTC 3 February 1991 from different runs: (a) CONTROL run; (b) NOLAT run.

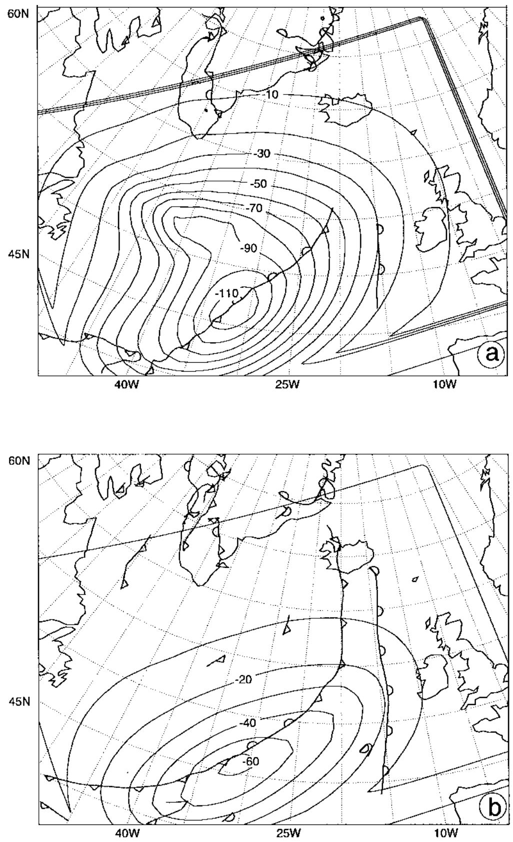

Fig. 9. Geopotential height field at 900 hPa associated with the lower boundary θ anomaly at 12 UTC 2 February: (a) CONTROL run; (b) RUN00.

front which is becoming wrapped around the low center (Bjørn Rosting, personal communication). To see how this relates to our question (2) above, we compare in Figs. 10a,b the contribution from UPV at the final time in three cases; CONTROL, ANA42 and RUN00. First, in Fig. 10a we see how much the UPV-anomaly is "in error" in the CONTROL run. This is seen to occur mainly between 45 and 55°N, i.e., well to the rear of the cyclone of interest, whereas the error near Iceland is very small. On the other hand, comparing the contribution from the UPV anomaly between CONTROL and RUN00, Fig. 10b, we see an underestimation of the cyclone by up to 40 gpm in RUN00. We suggest that this feature is a result of the vertical propagation of the initially low-level PV anomaly mentioned above. Hence, both the UPV field and its associated geopotential height field inherently consist of two features, the largest one being identical in all the runs due to its having been advected horizontally, uninfluenced by the low level flow, and a secondary feature being caused by vertical propagation of a PV anomaly related to the low-level cyclonic development early on. Since this initial development is too weak in RUN00, so is the secondary UPV feature at the final time.

4. Discussion

Despite the valuable insight gained in this study, there are a number of questions that may be raised regarding the methodology applied. One such

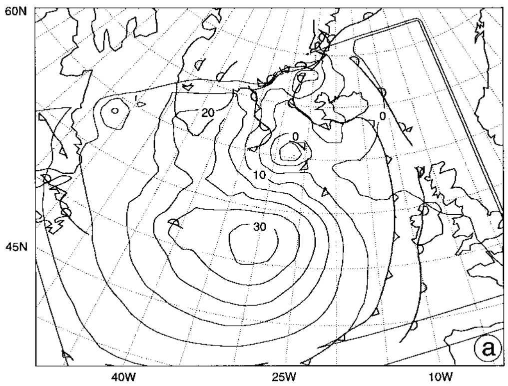

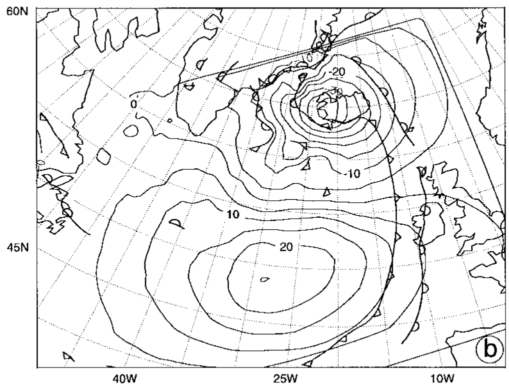

Fig. 10. Geopotential height difference fields at 900 hPa associated with the upper level PV anomaly at 12 UTC 3 February: (a) Difference between CONTROL run and ANA42 analysis; (b) Difference between CONTROL run and RUN00.

issue concerns the selection of the anomalies. Based on our preliminary results in KT, we started out by subjectively identifying three major positive anomalies that we focused on, i.e., UPV, LPV and surface θ'. It is to be expected that these three positive anomalies together overestimate the cyclone deepening, as positive anomalies induce deepening and negative anomalies induce filling. Hence, a fairly large residual term of opposite sign appears in Tables 1–5, containing all the contributions from negative anomalies. For this reason we have recomputed Table 1, including the four negative PV and *surface*-θ' anomalies UPVN1, UPVN2, LPVN and *surface*-θ'N, shown in Fig. 4. The result is presented in Table 6. We note that the contribution from the residual term has been drastically reduced. By including more anomalies the residual term could eventually be reduced to almost zero. The same exercise could easily be carried out for the other model simulations, but we have not done so.

Clearly, there are other cases in which a different choice of anomalies would be more suitable. Furthermore, in cases with less synoptic guidance it may not be clear how to select the relevant anomalies. Another related issue is how to define an anomaly once it has been selected. This issue can be split into two problems, i.e., how to define a mean field and how to select the anomalies from the perturbation field, in terms of grid points. Changing the definition of the mean field would implicitly change the perturbation field, and hence the anomalies, but the qualitative features of the results should not be affected greatly by this. We have chosen simply to use a time mean for the whole study period. This corresponds approximately to the life cycle of one extratropical cyclone, but a longer period can also be used, as suggested by DE.

Once a definition of the mean field has been decided upon, the problem of actually selecting the grid points that belong to a specific anomaly arises. Here it must be kept in mind that we only select grid points having a PV-perturbation of the same sign (either positive or negative), when we define a PV-anomaly. If the selected anomaly has a very small spatial extent, there will be surrounding grid points having a PV-perturbation of the same sign. Then, the result will be quite sensitive to small changes in the spatial extent. On the other hand, if the selected area is too large it may contain contributions from another anomaly of the same sign. As a compromise we have carefully selected large enough areas for each anomaly that the sensitivity is reduced, while still not extending over another anomaly of the same sign.

We have not shown any results concerning the upper boundary θ'. This is due to our assumption that anomalies there will not contain any significant meteorological signature, since the upper boundary lies entirely within the stratosphere. Independent calculations support this view and show that this is typically a small term.

In this study we have focused mainly on the instantaneous "forcing" imposed by the PV-anomalies. But, as pointed out by Stoelinga

Table 6. *As in Table 1, except P denotes positive anomalies, while N refers to negative anomalies*

Contributions to geopotential height in 42-h analysis							
Date/time	2/00	2/06	2/12	2/18	3/00	3/06	3/12
total	967	915	852	751	668	568	444
mean	1051	1009	980	918	851	765	720
perturbation	−84	−94	−128	−167	−183	−197	−276
UPVP	−35	−91	−82	−102	−108	−118	−181
UPVN1	41	62	64	96	142	45	52
UPVN2	9	15	16	9	19	28	38
LPVP	−35	−45	−96	−133	−177	−173	−156
LPVN	32	46	54	58	83	71	32
surface-θ'P	−73	−61	−81	−75	−67	−39	−42
surface-θ'N	4	6	8	11	22	29	27
res. + error	−27	−27	−11	−31	−98	−41	−42

(1996), there is a continuous interaction between the different portions of the PV-field. For instance, we saw in Subsection 3.3.4 how the *surface*-θ' anomaly played a crucial rôle in pre-conditioning the cyclone, hence allowing the subsequent merging between the low-level and upper-level anomalies. This non-linear effect might easily be overlooked if one were to look exclusively at Table 1, where we see that at 12 UTC 2 February, as well as at subsequent times, the contribution from *surface*-θ' to the cyclone depth was smaller than those of UPV and LPV.

Besides helping to understand explosive cyclone dynamics, PV inversion may conceivably have applications related to weather forecasting or analysis (Mansfield, 1994). For instance, if an error in a first-guess is known to be due to a particular feature at either the surface, low levels or upper levels, one way to correct it may be to modify the corresponding PV field, rather than the mass field, the advantage of using PV being that the three-dimensional aspect of the correction would be inherently taken care of.

5. Summary and conclusions

We have investigated an explosive synoptic-scale cyclone in the North Atlantic in the framework of potential vorticity (PV). Following a method recently developed by Davis and Emanuel (1991) we first identified a few distinct anomalies in the PV field. By successively inverting parts of the PV field, we then quantified the contributions from these anomalies to the geopotential field. Despite the non-linearity of PV, the contributions add up quite well, due to the particular procedure employed, suggested by Davis (1992). The inversions were performed on both data from ECMWF analysis and on data from different simulations, using the HIRLAM model. These simulations were previously described by Kristjánsson and Thorsteinsson (1995), where preliminary, qualitative PV diagnostics were presented. The results obtained here support the main conclusions from that study and at the same time put them on a more firm, quantitative footing. Our main findings from this investigation are as follows.

- The PV inversion methodology of Davis and Emanuel (1991) seems suitable for quantifying the contributions from different sources to the total geopotential field associated with the 2–3 February 1991 explosive cyclone near Iceland.
- An upper-level PV anomaly that contributed significantly to the final cyclone deepening phase has been shown to be mainly a separate entity advected by the upper-level flow, but to be partly due to vertical propagation of the PV from lower layers.
- The inversion results support the previous conclusion that insufficient surface baroclinicity early on was probably the main reason why many operational forecasts failed to predict the deepening of the explosive cyclone.
- In the case studied here, an area of negative PV rendered the inversions inaccurate there. Another consequence of the negative PVs was that we found convergence problems initiating in this area when fine horizontal grid resolution was used. The problem was solved by using a coarser resolution and then interpolating back to the original resolution.

• There is some arbitrariness in specifying and defining the anomalies, but this has been reduced by using consistent selection criteria.

6. Acknowledgements

This research has been supported by the Science Fund of the Icelandic Research Council. We wish to thank Dr. Christopher A. Davis, NCAR, for helpful advice and for kindly supplying some of the software for computing the PV inversions. Thanks are also due Sven Th. Sigurdsson, University of Iceland, for advice on numerical problems and Vidar Erlingsson for help in preparing the figures.

REFERENCES

Charney, J. G. 1955. The use of primitive and balance equations. *Tellus* **7**, 22–26.

Davis, C. A. 1992. Piecewise potential vorticity inversion. *J. Atmos. Sci.* **49**, 1397–1411.

Davis, C. A. and Emanuel, K. A. 1991. Potential vorticity diagnostics of cyclogenesis. *Mon. Wea. Rev.* **119**, 1929–1953.

Davis, C. A., Stoelinga, M. T. and Kuo, Y.-H. 1993. The integrated effect of condensation in numerical simulations of extratropical cyclogenesis. *Mon. Wea. Rev.* **121**, 2309–2330.

Ertel, H. 1942. Ein neuer hydrodynamischer Wirbelsatz. *Meteor. Zeits.* **59**, 271–281.

Grønås, S. 1995. The seclusion intensification of the New Year's day storm 1992. *Tellus* **47A**, 733–746.

Gustafsson, N. (ed.), 1993. Hirlam 2 final report. *HIRLAM Technical Report No. 9*, 126 pp.

Hakim, G. J., Keyser, D. and Bosart, L. F. 1996. The Ohio Valley wave-merger cyclogenesis event of 25–26 January 1978. Part II. Diagnosis using quasigeostrophic potential vorticity inversion. *Mon. Wea. Rev.* **124**, 2176–2205.

Holton, J. R. 1992. *An introduction to dynamic meteorology*. 3rd edition. International Geophysics Series, Vol.48, Academic Press, 511 pp.

Hoskins, B. J., McIntyre, M. E. and Robertson, A. W. 1985. On the use and significance of isentropic potential vorticity maps. *Quart. J. Roy. Meteor. Soc.* **111**, 877–946.

Hoskins, B. J. and Berrisford, P. 1988. A potential vorticity perspective of the storm of 15–16 October 1987. *Weather* **43**, 122–129.

Kristjánsson, J. E. and Thorsteinsson, S. 1995. The structure and evolution of an explosive cyclone near Iceland. *Tellus* **47A**, 656–670.

Mansfield, D. 1994. The use of potential vorticity in forecasting cyclones. Operational aspects. *The life cycle of extratropical cyclones,* vol. III, Symposium Proceedings, Bergen, Norway, 326–331.

Reed, R. J. 1955. A study of a characteristic type of upper-level frontogenesis. *J. Met.* **12**, 542–552.

Reed, R. J., Stoelinga, M. T. and Kuo, Y.-H. 1992. A model-aided study of the origin and evolution of the anomalously high potential vorticity in the inner region of a rapidly deepening marine cyclone. *Mon. Wea. Rev.* **120**, 893–913.

Rossby, C.-G. 1940. Planetary flow patterns in the atmosphere. *Quart. J. Roy. Meteor. Soc.* **66**, suppl., 68–87.

Shapiro, M. A. 1970. On the applicability of the geostrophic approximation to upper-level frontal-scale motions. *J. Atmos. Sci.* **27**, 408–420.

Stoelinga, M. T. 1996. A potential vorticity-based study on the role of diabatic heating and friction in a numerically simulated baroclinic cyclone. *Mon. Wea. Rev.* **124**, 849–874.

Uccellini, L. W. 1990. Processes contributing to the rapid development of extratropical cyclones. In: *Extratropical cyclones.* The Erik Palmén Memorial Volume (ed.C. Newton and E. Holopainen), AMS, Boston, 81–105.

Wernli, H. and Davies, H. C. 1997. A Lagrangian-based analysis of extratropical cyclones. I: The method and some applications. *Quart. J. Roy. Meteor. Soc.* **123**, 467–489.

Wu, C.-C. and Emanuel, K. A. 1995a. Potential vorticity diagnostics of hurricane movement. Part I. A case study of Hurricane Bob (1991). *Mon. Wea. Rev.* **123**, 69–92.

Wu, C.-C. and Emanuel, K. A. 1995b. Potential vorticity diagnostics of hurricane movement. Part II. Tropical Storm Ana (1991) and Hurricane Andrew (1992). *Mon. Wea. Rev.* **123**, 93–109.